Efficiency Optimization of Dual Active Bridge DC–DC Converter with Triple Phase-Shift Control

Garry Jean-Pierre
Center for Sustainable Electrical Energy Systems
University of Wisconsin-Milwaukee (UWM)
Milwaukee, USA
jeanpie4@uwm.edu

Necmi Altin
Dept. of Electrical – Electronics Engineering
Faculty of Technology
Gazi University
Ankara, Turkey
naltin@gazi.edu.tr

Ahmad El Shafei
Center for Sustainable Electrical Energy Systems
University of Wisconsin-Milwaukee (UWM)
Milwaukee, USA
aie@uwm.edu

Adel Nasiri
Center for Sustainable Electrical Energy Systems
University of Wisconsin-Milwaukee (UWM)
Milwaukee, USA
nasiri@uwm.edu

***Abstract*—The primary purpose of this paper is to obtain accurate analytical expressions of the dual active bridge (DAB) converter under the three-degree of freedom control technique. This technique, known as triple phase-shift (TPS) modulation, is utilized for the efficiency optimization of different operating zones and modes of the DAB. Three operating zones and modes have been retained to analyze the converter. Depending on the operating regions and due to the high nonlinearity of the obtained expressions, two optimization techniques have been used. The offline particle swarm optimization (PSO) method is utilized in local optimization (LO) and results in a numerical value. The Lagrange Multiplier (LM) is utilized in global optimization (GO) and results in a closed form expression. In the case of LO, the optimal duty cycles that minimize the power loss are not the optimal values for the minimum root-mean-square (RMS) current or peak current stress. Conversely, in the case of GO, the optimal duty cycles minimize the RMS, peak current and power loss at the same time for the entire power range. Detailed analyses and simulation results from MATLAB/Simulink are given to prove the effectiveness of the proposed method.**

Keywords—DAB, Lagrange Multiplier, loss optimization, PSO, TPS

I. INTRODUCTION

Due to capability of the DAB converter to auto-adjust the power flow in both directions, operate under wide voltage gain ratios and achieve zero-voltage-switching (ZVS), it has been widely used in many applications, including energy storage systems, micro-grids, solid state transformers, power electronic traction transformers and on-board chargers for electrical vehicles [1]. While DAB is a popular technology, there are many challenges to overcome. The high circulating current, which is analogous to reactive power in power system applications, does not participate in the power transfer of the converter. It is simply a heat source that affects the conduction and copper losses and eventually decreases the efficiency of the converter. Loss of ZVS is another issue that impacts the switching loss of the DAB [2]. Numerous modulation methods have been proposed in order to improve the performance of DAB converters. They can mainly be categorized into four techniques based on the degree of control freedom. The most common method is the single phase-shift (SPS), which uses only one control freedom to regulate the output power flow of the DAB [3]. In SPS control, the switch pairs in both full bridges are gated to obtain phase-shifted square waves with 50% duty cycle ratio. Only the phase-shift among the bridges is controlled. Adjusting the phase-shift between the primary and the secondary voltage results in the leakage inductor of the transformer changing to enable power flow direction and magnitude [4]. To increase the control flexibility of the DAB, extended phase-shift (EPS) [5] and dual phase-shift (DPS) [6] modulation schemes have been studied. In the EPS method, the switch pairs in one full bridge are switched with an inner phase-shift ratio. This enables the AC output voltage of one bridge to be a three-level wave while the other one is a two-level 50% square wave [5]. Both methods contain two control variables. In the EPS method, the duty ratio of one full bridge is considered in addition to the phase-shift, while in the DPS method, both full bridges use an inner equal phase-shift ratio in addition to the phase-shift. Comparatively, while both methods maintain the same operating conditions of the two bridges, even while the converter changes power flow direction, the implementation of the DPS is easier than the EPS method. The triple phase-shift (TPS) modulation strategy [7] regulates the duty ratios of the two full bridges and the phase-shift ratio independently. The SPS, EPS and DPS controls are all special cases of TPS. The same power flow can be obtained with different phase-shift and duty cycle values. Therefore, multiple optimization targets have been formed using the optimal TPS variables. In [8], the maximum fundamental active power was considered as the objective function. In [9], the current amplitude of the fundamental component was to be minimized. In [10], the minimum fundamental reactive power is used. In [11]- [13], the minimum current stress was taken into consideration and in [14] and [15] the RMS current was chosen as the objective function to be minimized. While these optimization targets are aimed at improving the overall performance and efficiency of the DAB, the maximum efficiency of the converter is not guaranteed. In order to obtain the maximum efficiency of the DAB, this paper is proposing the overall power loss of the converter as the target function to be minimized. Analyses and simulation studies using MATLAB /Simulink have been carried out to prove the effectiveness of the proposed methodology.

The paper is organized as follows. Section II presents a description of the DAB analysis and its operating power zones. In Section III, particular calculation and analysis of the DAB converter overall power losses are performed, and the manipulated variables to control the required power flow and

978-1-7281-5826-6/20/$31.00 ©2020 IEEE

minimize the DAB converter total power losses for each zones are obtained. The optimization methods and control structure are in Section IV. Section V presents a summary of the simulation results to validate the theoretical proposal.

II. DAB Converter Analysis

The DAB converter and the corresponding switching sequences, key voltages and current waveforms under TPS conditions are shown in Fig. 1, and Fig. 2, respectively. The DAB contains two full bridges, operating as a DC-AC and AC-DC converter connected via a high-frequency transformer. When the TPS control modulation scheme is used to regulate the DAB, the analyses can be divided into six regions. However, for the purpose of calculating the total power loss of the converter, three zones are retained and defined with their respective boundary conditions. In zone 1, which is analogous to the low power region, the power flow follows the following constraint $0 \leq D_2 \leq \varphi \leq D_1 \leq 1$. Zone 2, which is the connotation for the medium power area, is defined by $0 \leq D_2 \leq D_1 \leq \varphi \leq 1$. Zone 3 is the high power region with $0 \leq D_1 \leq D_2 \leq \varphi \leq 1$ as the boundary condition. The different zones of operation are depicted in Fig. 3. D_1 and D_2 are the duty cycles of the first and second converters, respectively, and φ is the phase shift between V_1 and V_2. The DAB converter efficiency expression will be formulated in terms of the semiconductor and high frequency transformer losses in order to minimize the total power loss. Detailed and accurate analysis of each component of the total loss is presented for each of the three zones.

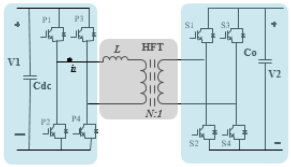

Fig. 1 Dual active bridge

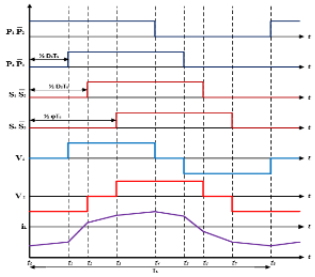
Fig.2 Gates, voltages and current

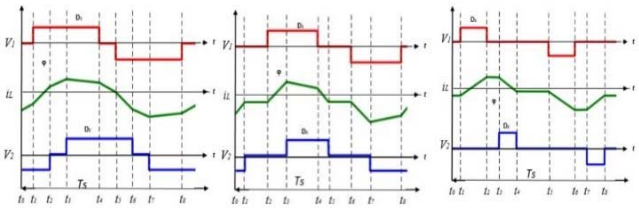

(a) (b) (c)

Fig. 3 Voltages and current waveforms (a) Zone 3, (b) Zone 2 (c) Zone 1

III. Analysis Of The DAB Converter Power Losses And Efficiency

In order to minimize the total power loss, the efficiency of the DAB converter will be formulated in terms of the four main losses: conduction, switching, winding and core losses based on the manipulated variables D_1, D_2 and φ. Therefore, detailed analyses are carried out for each component of the DAB and for each zone of operation.

A. Semiconductor Power Losses

In the semiconductors, two types of losses are considered for this analysis: conduction and switching. Conduction losses are formulated for each semiconductor device, transistor and diode, based on current and voltage waveforms for each interval, as demonstrated in Fig. 2. V_{on} represents the transistor voltage during on state, V_d is the diode forward voltage drop and $I_{L_{t_x \to t_y}}$ is the current during the conduction intervals. Switching losses are calculated for each switching event, based on Fig. 2. V_x and V_y are the voltages at turn-on and turn-off, respectively. i_{Lpi} is the peak current during each switching event, t_f is the fall time and C_{dev} is the snubber capacitor of the transistor. Due to fact that the converter can operate in either hard-switching or soft-switching, the ZVS constraint is established when the i_l zero crossing is within the time interval where V_1 and V_2 have opposite polarities. When the converter is operating under soft-switching, only turn-off losses are calculated. When the converter is working under hard-switching, turn-on losses are also considered. Tables I – X summarize the derived expressions for obtaining the switching and conduction losses for each zone of operation.

TABLE I. Conduction And Switching Loss General Expressions

Conduction Losses (P_{cond})	Switching Losses (P_{sw})
$P_{cond} = \frac{1}{T_s}\left(\int_{t_x}^{t_y} \lvert I_{Lt_{x\_}t_y} \rvert V_{on}\, dt + \int_{t_x}^{t_y} \lvert I_{Lt_{x\_}t_y} \rvert V_d\, dt\right)$	$P_{sw} = \frac{1}{2} V_x i_{Lpi} t_f f_s + \frac{1}{2} C_{dev} V_y^2 f_s$

TABLE II. DAB Currents At Each Switching Events - Zone 3

$i_{lp1} = -I_{lp}(t_0) = I_{lp}(t_4) = -I_{lp}(t_8) = \frac{V_1(1-D_1) + V_2(\Phi + D_2 - 1)}{4Lf_s}$	$i_{lp2} = -I_{lp}(t_1) = I_{lp}(t_5) = \frac{V_1(D_1 - 1) + V_2(1 + \Phi - 2D_1 + D_2)}{4Lf_s}$
$i_{lp3} = I_{lp}(t_2) = -I_{lp}(t_6) = \frac{V_1(-1 - D_1 + 2D_2) + V_2(1 + \Phi - D_2)}{4Lf_s}$	$i_{lp4} = I_{lp}(t_3) = -I_{lp}(t_7) = \frac{V_1(-1 - D_1 + 2\Phi) + V_2(1 + \Phi - D_2)}{4Lf_s}$

TABLE III. DAB Average Currents For Each Interval - Zone 3

$I_{L_{t_0\_t_1}} = \frac{V_1(D_1 - 1) - V_2(\Phi - 2D_1 + D_2 - 1)}{4Lf_s}$	$I_{L_{t_4\_t_5}} = \frac{V_1(1 - D_1) - V_2(1 + \Phi - 2D_1 + D_2)}{4Lf_s}$
$I_{L_{t_1\_t_2}} = \frac{V_1(D_1 - 2D_2 - 1) - V_2(\Phi - D_2 - 1)}{4Lf_s}$	$I_{L_{t_5\_t_6}} = \frac{V_1(1 + D_1 - 2D_2) - V_2(1 + \Phi - D_2)}{4Lf_s}$
$I_{L_{t_2\_t_3}} = \frac{V_1(D_1 - 2\Phi - 1) - V_2(\Phi - D_2 - 1)}{4Lf_s}$	$I_{L_{t_6\_t_7}} = \frac{V_1(1 + D_1 - 2\Phi) - V_2(1 + \Phi - D_2)}{4Lf_s}$
$I_{L_{t_3\_t_4}} = \frac{V_1(1 - D_1) - V_2(1 + \Phi + D_2)}{4Lf_s}$	$I_{L_{t_7\_t_8}} = \frac{V_1(D_1 - 1) - V_2(-1 + \Phi + D_2)}{4Lf_s}$

TABLE IV. Zone 3 Conduction And Switching Losses

$P_{sw} = \frac{V_1 t_f \lvert V_1 - V_2 + \Phi V_2 + D_1 V_1 - 2D_2 V_1 - D_2 V_2 \rvert + V_2 t_f \lvert V_1 - V_2 + \Phi V_2 - D_1 V_1 + D_2 V_2 \rvert}{8L}$
$P_{cond} = 12 V_f L f_s \left(\begin{array}{l} \lvert(\Phi - 1)(V_1(\Phi - D_1) + D_2 V_2)\rvert + D_1 \lvert -V_1(D_2 + D_1) + V_2(2\Phi + D_2 - 2D_1 - 2)\rvert \\ + D_2 \lvert (V_2(D_1 - D_2) + V_1(D_1 - \Phi)\rvert + \Phi \lvert (V_2(1 + D_2 - \Phi) + V_1(\Phi - D_1 + D_2 - 1))\rvert \\ + R_{ds} V_1^2 (2D_1^3 - 3D_1^2 + 1) + R_{ds} V_2^2 (2(D_2 - \Phi)^3 - 3(D_2 + \Phi)^2 + 1) \end{array} \right)$ $= \frac{+ 2R_{ds} V_1 V_2 (2(D_1^3 - D_2^3 - \Phi^3) + 3D_1(D_2^2 - D_1 D_2 + \Phi^2 - D_1\Phi) + 3(D_1 - D_2)^2 + 3\Phi(\Phi - D_1) - 1)}{24 L^2 f_s^3}$

TABLE V. DAB Currents At Each Switching Events - Zone 2

$i_{lp1} = -I_{lp}(t_0) = I_{lp}(t_4) = -I_{lp}(t_8) = \frac{V_1(1-D_1) + V_2(\Phi + D_2 - 1)}{4Lf_s}$	$i_{lp3} = I_{lp}(t_3) = -I_{lp}(t_7) = \frac{V_1(-1 - D_1 + 2D_2) + V_2(1 + \Phi - D_2)}{4Lf_s}$
$i_{lp2} = -I_{lp}(t_1) = -I_{lp}(t_2) = I_{lp}(t_5) = I_{lp}(t_6) = \frac{V_1(D_1 - 1) + V_2(1 + \Phi - 2D_1 + D_2)}{4Lf_s}$	

TABLE VI. DAB AVERAGE CURRENTS FOR EACH INTERVAL- ZONE 2

$I_{L_{t_0\_t_1}} = \frac{V_1(D_1-1)+V_2(1+D_2-\Phi)}{4Lf_s}$	$I_{L_{t_4\_t_5}} = \frac{V_1(1-D_1)+V_2(\Phi-D_2-1)}{4Lf_s}$
$I_{L_{t_1\_t_2}} = \frac{V_1(D_1-1)+V_2(D_2-\Phi+1)}{4Lf_s}$	$I_{L_{t_5\_t_6}} = \frac{V_1(1-D_1)+V_2(\Phi-D_2-1)}{4Lf_s}$
$I_{L_{t_2\_t_3}} = \frac{V_1(2\Phi-D_1-1)-V_2(\Phi-1-D_2)}{4Lf_s}$	$I_{L_{t_6\_t_7}} = \frac{V_1(1+D_1-2\Phi)+V_2(1+\Phi-D_2)}{4Lf_s}$
$I_{L_{t_3\_t_4}} = \frac{V_1(1-D_1)+V_2(-1+\Phi+D_2)}{4Lf_s}$	$I_{L_{t_7\_t_8}} = \frac{V_1(D_1-1)+V_2(-1+\Phi+D_2)}{4Lf_s}$

TABLE VII. ZONE 2 CONDUCTION AND SWITCHING LOSSES

$P_{SW} = \frac{\lvert\left(V_1 t_f(V_1(1-D_1)+V_2(D_2+\Phi-1))\right)\rvert + \lvert\left(V_2 t_f(V_2(1-\Phi+D_2)+V_1(D_1-1))\right)\rvert}{8L}$
$P_{cond} = \frac{\begin{array}{c}12V_f Lf_s\left(\lvert(\Phi-1)(V_1(\Phi-D_1)-D_2V_2)\rvert - D_1^2\left\lvert V_1\left(1-\frac{\Phi}{D_1}\right)\right\rvert + D_2^2\lvert V_2\rvert + \Phi\left\lvert\begin{matrix}V_1(\Phi-1)\\+V_2(1+D_2-\Phi)\end{matrix}\right\rvert\right)\\+R_{ds}V_2^2(2(\Phi-D_2)^3-3(\Phi-D_2)^2+1)+R_{ds}V_1^2(2D_1^3-3D_1^2+1)\\+2R_{ds}V_1V_2(3D_2^2+3\Phi^2-4\Phi^3-3D_1(D_2^2+\Phi^2)+3D_1^2(D_2-\Phi+3)-3D_1(D_2-\Phi)-1)\end{array}}{24L^2f_s^3}$

TABLE VIII. DAB CURRENTS AT EACH SWITCHING EVENTS - ZONE 1

$\boldsymbol{i_{lp1} = -I_{lp}(t_0) = I_{lp}(t_4) = -I_{lp}(t_8)} = \frac{V_1(1-D_1)+V_2(\Phi+D_2-1)}{4Lf_s}$	$\boldsymbol{i_{lp3} = -I_{lp}(t_3) = I_{lp}(t_7)} = \frac{V_2(1-2D_1+\Phi+D_2)+V_1(D_1-1)}{4Lf_s}$
$\boldsymbol{i_{lp2} = -I_{lp}(t_1) = -I_{lp}(t_2) = I_{lp}(t_5) = I_{lp}(t_6)} = \frac{V_2(1+D_2-\Phi)+V_1(D_1-1)}{4Lf_s}$	

TABLE IX. DAB AVERAGE CURRENTS FOR EACH INTERVAL - ZONE 1

$I_{L_{t_0\_t_1}} = \frac{V_1(D_1-1)+V_2(1-\Phi+D_2)}{4Lf_s}$	$I_{L_{t_4\_t_5}} = \frac{V_1(1-D_1)-V_2(1-\Phi+D_2)}{4Lf_s}$
$I_{L_{t_1\_t_2}} = \frac{V_1(D_1-1)+V_2(1-\Phi+D_2)}{4Lf_s}$	$I_{L_{t_5\_t_6}} = \frac{V_1(1-D_1)-V_2(1-\Phi+D_2)}{4Lf_s}$
$I_{L_{t_2\_t_3}} = \frac{V_1(D_1-1)+V_2(1+\Phi-2D_1+D_2)}{4Lf_s}$	$I_{L_{t_6\_t_7}} = \frac{V_1(1-D_1)-V_2(1+\Phi-2D_1+D_2)}{4Lf_s}$
$I_{L_{t_3\_t_4}} = \frac{V_1(1-D_1)-V_2(\Phi+D_2-1)}{4Lf_s}$	$I_{L_{t_7\_t_8}} = \frac{V_1(D_1-1)-V_2(\Phi+D_2-1)}{4Lf_s}$

TABLE X. ZONE 1 CONDUCTION AND SWITCHING LOSSES

$P_{SW} = \frac{\lvert V_1 t_f(V_1(1-D_1)+V_2(\Phi+D_2-1))\rvert + \lvert V_2 t_f(V_2(1+D_2-\Phi)+V_1(D_1-1))\rvert + 4C_{dev}f_sL(V_1^2+V_2^2)}{8L}$
$P_{cond} = \frac{\begin{array}{c}12\Phi V_f Lf_s\left(\lvert(V_2(1-D_1+D_2)+V_1(D_1-1))\rvert(1-D_1)+D_2\left\lvert\begin{matrix}\lvert V_2(\Phi-1)\rvert\\-\lvert V_2(1+D_2-\Phi)+V_1(D_1-1)\rvert\end{matrix}\right\rvert\right.\\\left.+\Phi\lvert(V_2(1+D_2-\Phi)+V_1(D_1-1))\rvert\right)\\+12V_f Lf_s\lvert V_2\rvert(D_2+D_1(D_1-D_2-\Phi-1)+\Phi)+R_{ds}V_2^2(2(\Phi-D_2)^3-3(D_2+\Phi)^2+1)\\+R_{ds}V_1V_2(6(D_1-D_2)^2-4D_1^3+6\Phi^2-6D_1D_2^2+6D_1^2D_2-6D_1\Phi^2+6D_1^2\Phi-6D_1\Phi-2)\\+R_{ds}V_1^2(1-3D_1^2+2D_1^3)\end{array}}{24L^2f_s^3}$

B. Transformer Power Losses

The transformer losses are the total sum of the core and winding losses. To obtain the winding loss, the RMS current is determined and both the skin and proximity effect are considered for calculating R_{eff}. Due to the non-sinusoidal waveform characteristic for the given applications, the Improved Generalized Steinmetz Equation (IGSE) [16] is used to obtain the closed form expression for the core loss. Tables XI - XIV show the derived expressions for the transformer losses. Table XV summarizes the average power expressions for each zones, efficiency and the sum of the winding, core, switching and conduction losses to compute the total power loss for the converter.

IV. OPTIMIZATION METHOD AND CONTROL STRUCTURE

The goal of the optimization is to minimize the total power loss for a given average power. The variables are D_1, D_2, and φ. The objective function, *f*, is the total power loss which needs to be minimized and the constraint, *g*, is the average power the converter should be able to provide. Two optimization methods have been used, the LM and the PSO. Due to the nonlinearity of the system, in certain power regions it is extremely difficult to obtain a closed loop form for the optimal degree of freedom. In such a case, the PSO is utilized to obtain an optimal numerical value for the degree of freedom. This case is also referred to as LO. However, in other power regions it is possible to obtain a closed loop form for the optimal degree of freedom. In this case the LM method is used for the constraint optimization problem of the DAB. This case is also referred to as GO. Contrary to the LO method, the GO method covers multiple target functions, such as peak current stress, RMS current and total power loss.

TABLE XI. TRANSFORMER LOSSES MAIN EQUATIONS

Winding Loss		Core Loss
$\boldsymbol{P_{W_{loss}}} = R_{eff}I_{rms}^2$	$R_{eff} = R_{dc}\left(\left(\frac{R_{ac}}{R_{dc}}\right) + G_r N_s\left(\left(\frac{1}{\pi^2 d_{litz}^4}\right) + N_l^2\frac{4M_l^2-1}{12H_w^2}\right)\right)$ $I_{rms} = \sqrt{\left(\sum_{(i=1)}^{8}\int_{ZAi}^{ZBi}(I(t)-I_{ave})dt\right)^2}$	$\boldsymbol{P_{core}} = \frac{1}{T_s}\int_0^{T_s} K_i\left\lvert\frac{dB(t)}{dt}\right\rvert^{\gamma}(\Delta B)^{\theta-\gamma}\,dt$ $K_i = \frac{2^{1-\theta}K_s\pi^{1-}}{\frac{1.7061}{+1.354}+0.2761}$

TABLE XII. CORE LOSS AND RMS CURRENT OF THE DAB - ZONE 3

RMS Current (I_{rms})	Core Loss (P_{core})
$I_{rms} = \frac{\sqrt{3}}{3}\frac{\left(\begin{array}{c}4V_1V_2(3D_1(D_1D_2+D_1\Phi-D_1-D_2^2+D_2+\Phi-\Phi^2)+3(D_2^3-D_2^2-\Phi^2)+2(\Phi^3-D_1^3)+1)\\+2V_1^2(3D_1^2-2D_1^3-1)+2V_2^2(2(D_2^3-\Phi^3)-6(D_2^2\Phi+D_2\Phi^2-D_2\Phi)+3(\Phi^2+D_2^2)-1)\end{array}\right)^{\frac{1}{2}}}{4Lf_s}$	$P_{core} = K_i(2B_m)^{\theta-}\left(\left(\frac{T_s}{2}-\frac{\Phi T_s}{2}\right)(B_m f_s)\ (2\ +4\ ) + \left(\frac{D_2T_s}{2}-\frac{D_1T_s}{2}\right)\left(\left(\frac{2B_m}{\frac{D_2T_s}{2}+\frac{T_s}{2}}\right)+\left(\frac{4B_m f_s}{D_2}\right)\right)\right.$ $\left.+\left(\frac{\Phi T_s}{2}-\frac{D_2T_s}{2}\right)\left(\ +\left(\frac{4B_m f_s}{\Phi}\right)\right)\right)$

TABLE XIII. CORE LOSS AND RMS CURRENT OF THE DAB - ZONE 2

RMS Current (I_{rms})	Core Loss (P_{core})
$I_{rms} = \frac{\sqrt{3}}{3}\frac{\left(\begin{array}{c}2V_1V_2(6(D_1^2\Phi-D_1^2D_2-D_1^2+D_1D_2^2+D_1D_2-D_1\Phi^2+D_1\Phi-D_2^2-\Phi^2)+4\Phi^3+2)\\+2V_1^2(3D_1^2-2D_1^3-1)+2V_2^2(2(D_2^3-\Phi^3)-6(D_2^2\Phi+D_2\Phi^2-D_2\Phi)+3(\Phi^2+D_2^2)-1)\end{array}\right)^{\frac{1}{2}}}{4Lf_s}$	$P_{core} = K_i(2B_m)^{\theta-}\left(\left(\begin{matrix}\frac{T_s}{2}\\-\frac{\Phi T_s}{2}\end{matrix}\right)(B_m f_s)\ \left(\begin{matrix}2\\+4\end{matrix}\right) + \left(\begin{matrix}\frac{\Phi T_s}{2}\\-\frac{D_1T_s}{2}\end{matrix}\right)\left(\left(\frac{2B_m}{\frac{\Phi T_s}{2}+\frac{T_s}{2}}\right)+\left(\frac{4B_m f_s}{\Phi}\right)\right)\right)$

TABLE XIV. CORE LOSS AND RMS CURRENT OF THE DAB - ZONE 1

RMS Current (I_{rms})	Core Loss (P_{core})
$I_{rms} = \frac{\sqrt{3}}{3}\frac{\left(\begin{array}{c}V_1V_2(4D_1^3+6(D_1^2D_2+D_2^2\Phi+D_1^2-D_1D_2^2-D_1D_2-D_1\Phi^2-D_1\Phi+D_2^2+\Phi^2)-2)\\-V_1^2(3D_1^2-2D_1^3-1)+V_2^2(2D_2^3-6D_2^2\Phi+3D_2^2+6D_2\Phi^2-6D_2\Phi-2\Phi^3+3\Phi^2-1)\end{array}\right)^{\frac{1}{2}}}{4Lf_s}$	$P_{core} = K_i(2B_m)^{\theta-}\left(\left(\frac{T_s}{2}-\frac{D_1T_s}{2}\right)(B_m f_s)\ (2\ +4\ )\right)$

TABLE XV. TOTAL LOSSES, AVERAGE POWER AND EFFICIENCY OF THE DAB

Average Power Transfer		Efficiency
Zone 3	$P_{ave} = \frac{V_1V_2(D_1(D_2+\Phi-1)-D_1^2-D_2^2+D_2-\Phi^2+\Phi)}{4Lf_s}$	$\boldsymbol{\eta} = \frac{P_{ave}-P_{Loss}}{P_{ave}}$
Zone 2	$P_{ave} = \frac{V_1V_2(D_2-\Phi^2+\Phi-D_1(D_2-\Phi+1))}{4Lf_s}$	Total Power Loss
Zone 1	$P_{ave} = \frac{V_1V_2(1-D_1)(D_2-D_1+\Phi)}{4Lf_s}$	$\boldsymbol{P_{loss}} = P_{W_{loss}}+P_{core}+P_{cond}+P_{sw}$

A. Lagrange Multiplier Method

Based on Lagrange optimization methodology, a Lagrange function is the combination of the objective function and the constraint multiplied by λ as formulated in (1).

$$\Lambda(D_1, D_2, \varphi, \lambda) = f(D_1, D_2, \varphi) + \lambda_g(D_1, D_2, \varphi) \quad (1)$$

The optimal solution of the constraint optimization is described by a set of equations of the gradient of the LM as written in (2) for the DAB. Although $\partial\Lambda/\partial\lambda = 0$ is part of $\nabla\Lambda = 0$, it does not reveal any new information because it is simply the constraint function, g, itself.

$$\nabla\Lambda = 0 \rightarrow \frac{\partial\Lambda}{\partial D_1} = 0 \;\&\; \frac{\partial\Lambda}{\partial D_2} = 0 \;\&\; \frac{\partial\Lambda}{\partial\varphi} = 0 \quad (2)$$

For each of the modes and power regions where GO is feasible, as summarized in Table XVI, the corresponding average power transferred and the objective function can be used to obtain the closed form expressions according to (1) and (2). This paper covers the case of $V_1>V_2$ for all three power regions. Similarly, the case for $V_1<V_2$ and $V_1=V_2$ can be derived. In zone 2, GO exists; therefore, the closed form expressions for minimizing the power loss can be obtained. For the sake of simplicity, the peak current stress (i_{lp1}) from Tables II, V and VIII is chosen as the objective function and the corresponding average power for zone 2 in Table XV is used. Substituting the per unit expressions as formulated in (3) into (1) and (2) yields the following closed form expressions for D_1 and D_2 as formulated in (4). The rated values of the power and the peak current are computed as follows: $P_r = \frac{V_1 V_2}{8Lf_s} \quad \& \quad I_r = \frac{V_2}{8Lf_s}$

$$\begin{cases} P_{ave_{pu}} = 2(D_2 - D_1 + \varphi - \varphi^2 - D_1 D_2 + D_1\varphi) \\ I_{lp_{pu}} = \frac{2V_1}{V_2}(1 - D_1) + (\Phi + D_2 - 1) \end{cases} \quad (3)$$

$$\begin{cases} D_1 = 2\varphi - \frac{\varphi}{\sqrt{\frac{V_1}{V_2}}} + \frac{1}{\sqrt{\frac{V_1}{V_2}}} - 1 \\ D_2 = \frac{3}{2}\varphi - \frac{V_1(\varphi-1)}{V_2\sqrt{\frac{V_1}{V_2}}} - 1 \end{cases} \quad \left(\frac{V_2V_1 - V_2^2}{V_1^2} < P_{Ave_{pu}} \le \frac{3V_2V_1 - V_2^2}{V_1^2}\right) \quad (4)$$

B. Particle Swarm Optimization Method

The flowchart of the offline PSO technique is presented in Fig. 4. This method is used for obtaining the optimal control variables for zones 1 and 3. The PSO formulation comprises two principal equations, as seen in (5) and (6), where X is defined as particle positions (TPS variables) and V is the particle velocity that is used to modify the particle position X for every iteration. P_{best} is the best remembered individual particle position and G_{best} is the best remembered swarm position. k is the iteration index, c_1 and c_2 are positive constants and r_1 and r_2 are two randomly generated numbers, such that $0 \leqslant r_1, r_2 \leqslant 1$ [17].

$$X_i^{k+1} = X_i^k + V_i^{k+1} \quad (5)$$

$$V_i^{k+1} = wV_i^k + C_1 r_1\left(P_{best_i}{}^k - X_i^k\right) + c_2 r_2(G_{best}^k - X_i^k) \quad (6)$$

C. Control Structure

The optimal closed loop control is shown in Fig. 5. This figure depicts the case $V_1>V_2$. Similarly, for the other modes of operation the corresponding data can be added based on table XVI. The phase-shift φ_1 is generated by a PI controller and is fed into the optimal control variables generation block to estimate the average power transferred from the first bridge to the second bridge. Based on the estimated average power, the operating zone is then determined. The optimal D_{1opt} and D_{2opt} are calculated either from (4) or are chosen from the PSO look up table (LUT). Fig. 6 shows the optimization trajectories for obtaining the optimal degree of freedom: (a) – (d) for zone 3, (e) – (h) for zone 2, (i) – (l) for zone 1.

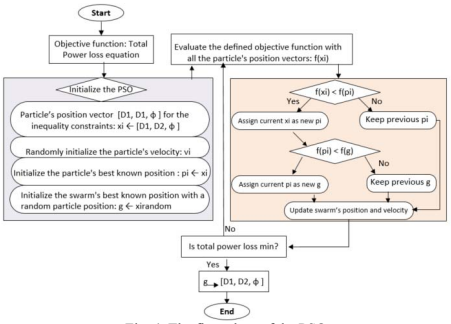

Fig. 4. The flow chart of the PSO

TABLE XVI. OPTIMIZATION METHOD BASED ON MODES OF OPERATIONS AND POWER REGIONS

	Power Regions		
Modes	Zone 1	Zone 2	Zone 3
$V_1<V_2$	GO→ LM	LO→ PSO	LO→ PSO
$V_1=V_2$	GO→ LM	GO(Ilp, Irms) → LM & LO (Ploss) → PSO	LO→ PSO
$V_1>V_2$	LO→PSO	GO→ LM	LO→ PSO

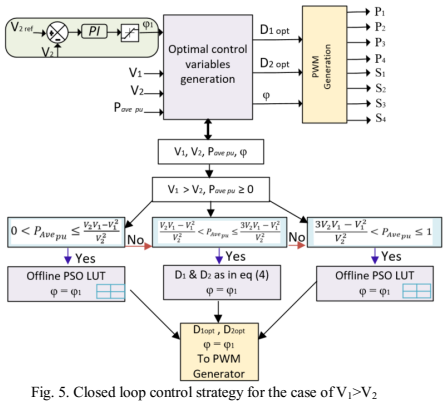

Fig. 5. Closed loop control strategy for the case of $V_1>V_2$

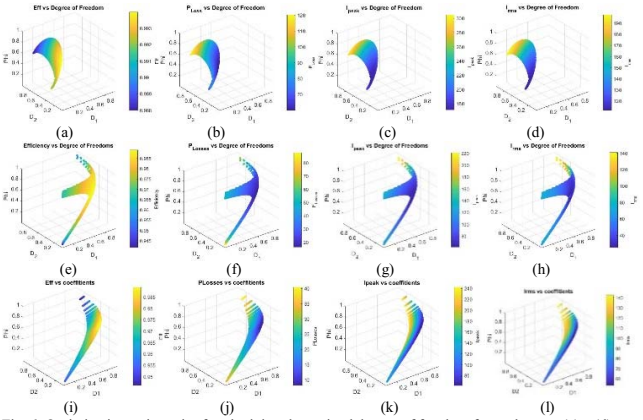

Fig. 6. Optimization trajectories for obtaining the optimal degree of freedom for each zone. (a) – (d) zone 3, (e) – (h) zone 2, (i) – (l) zone 1.

V. SIMULATION RESULTS

Utilizing the total power loss equation from Table XV, two optimization algorithms can be used. PSO is used when the

optimal values that minimize the power loss are different from the optimal values that minimize the RMS or the peak current. The LM is used for obtaining a closed form expression for the optimal degree of freedom when there is an optimal value that minimizes the power loss, the RMS and the peak current simultaneously. The simulation of the DAB was carried out based on Fig. 3. Table XVII summarizes the effectiveness of the control strategy. The simulation results for all three zones are presented in Fig. 7. – 9.

Additionally, the SPS is compared to the proposed TPS method in order to validate the effectiveness of the proposed technique. As seen in Table XVII, for the high power zone the efficiency is increased by 0.4% while the RMS current is decreased by 0.5 A. This case can be predicted from Table XVI where it shows for zone 3 only one objective function can be minimized. For the medium power range, the LM method is used to minimized multiple objective functions at the same time. It can be seen that the efficiency is increased by 1.25% and the RMS current is decreased by 16.3 A.

The most significant improvement of the efficiency happens for the low power zone: it is increased by 14.1%. In this zone of operation, the optimal control variables for the maximum efficiency also minimize the RMS current by 36.8 A. While it is expected that RMS current will be lower for the optimum variables for power loss minimization in the low power zone, these are not necessarily the optimum variables for the RMS current.

Lower RMS current can be achieved while compromising the efficiency. Such a case was evaluated in the simulation and the RMS current was further decreased by 40.7 A while the efficiency was increased by 12.7%. As summarized in Table XVII, utilizing the TPS control strategy based on the formulated equations results in an increased efficiency of the converter. The switches parameters were extracted from the C3M0060065J Silicon Carbide Power MOSFET C3M™ MOSFET Technology from CREE.

TABLE XVII. SUMMARY OF THE SIMULATION RESULTS WHICH ILLUSTRATE THE EFFECTIVENESS OF TPS VS. SPS

	High Power (Zone 3)		Medium Power (Zone 2)		Low Power (Zone 1)	
Control Method	TPS	SPS	TPS	SPS	TPS	SPS
RMS Current (A)	59.8	60.3	38.2	54.5	14.1	50.9
Input Power (kW)	2.569	2.569	1.53	1.538	0.303	0.354
Output power (kW)	2.5	2.5	1.5	1.5	0.3	0.3
Efficiency (%)	97.4	97	98.3	97.05	98.9	84.8

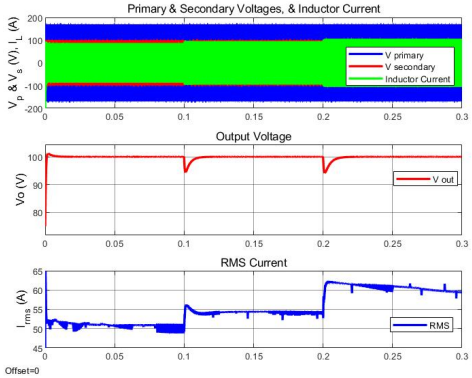

(a)

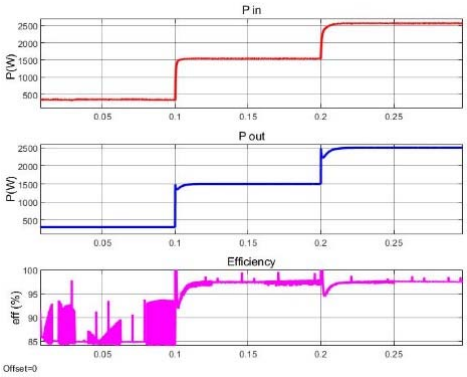

(b)

Fig. 7. Simulation results of the DAB under SPS for the three power zones (a) primary and secondary voltages, leakage current, output voltage and RMS current (b) Input and output power, and efficiency.

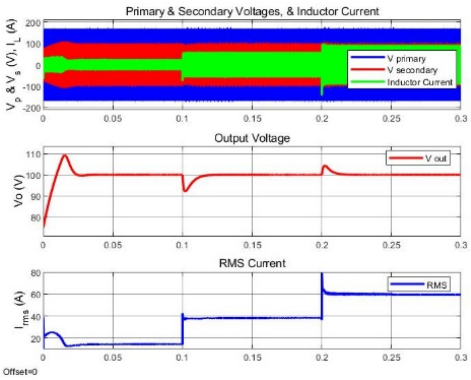

(a)

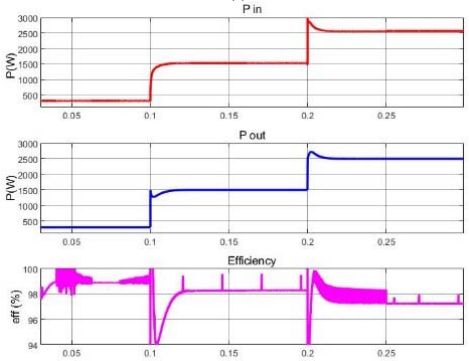

(b)

Fig. 8. Simulation results of the DAB under TPS for the three power zones (a) primary and secondary voltages, leakage current, output voltage and RMS current (b) Input and output power, and efficiency.

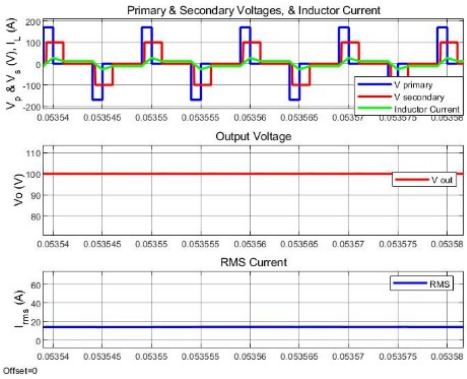

(a)

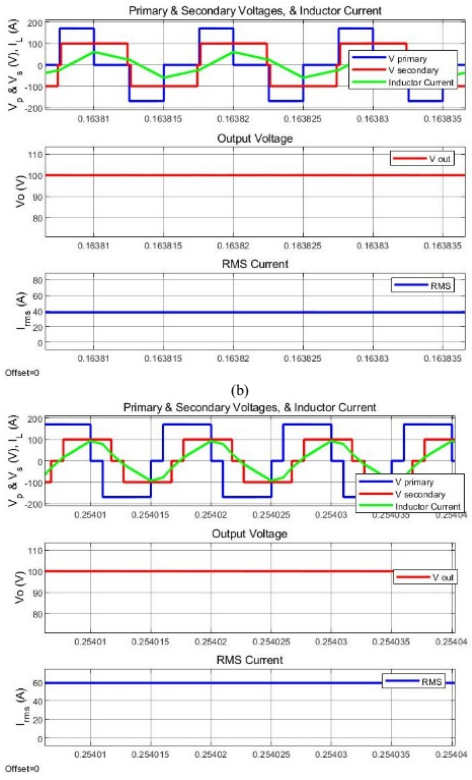

Fig. 9. Exploded view of the primary and secondary voltages under TPS for the three power zones (a) Zone 1 (b) Zone 2 (c) Zone 3

VI. Conclusions

This paper presents detailed analyses of obtaining the total power loss utilizing the TPS method resulting in the optimal control and maximum efficiency of the DAB converter. The methodology to calculate the DAB losses (including conduction, switching, winding and core losses) and efficiency was developed for three zones and modes of operation. The buck mode analysis and simulation results are presented for each zone. The analysis and summary of the simulation results from Table XVII demonstrate the effectiveness of the study. It is seen from the results that the efficiency of the converter is greatly improved for zone 1 and 2 by using the proposed method.

Acknowledgment

This material is based upon work supported by the National Science Foundation under Grant No. 1650470. Any opinions, findings, and conclusions or recommendations expressed in this material are those of the author(s) and do not necessarily reflect the views of the National Science Foundation.

References

[1] R. W. De Doncker, D. M. Divan, and M. H. Kheraluwala, ‘‘A threephase soft-switched high power density DC/DC converter for high power applications,’’ in Proc. Conf. Rec. IEEE Ind. Appl. Soc. Annu. Meeting, vol. 1, Oct. 1988, pp. 796–805.

[2] S. Shao, H. Chen, X. Wu, J. Zhang and K. Sheng, "Circulating Current and ZVS-on of a Dual Active Bridge DC-DC Converter: A Review," in IEEE Access, vol. 7, pp. 50561-50572, 2019.

[3] S. Inoue and H. Akagi, “A bidirectional isolated dc-dc converter as a core circuit of the next-generation medium-voltage power conversion system,” IEEE Trans. Power Electron., vol. 22, no. 2, pp. 535–542, Mar. 2007.

[4] F. Krismer and J. W. Kolar, “Accurate small-signal model for the digital control of an automotive bidirectional dual active bridge,” IEEE Trans. Power Electron., vol. 24, no. 12, pp. 2756–2768, Dec. 2009.

[5] G. G. Oggier, G. O. Garcia, and A. R. Oliva, “Modulation strategy to operate the dual active bridge dc-dc converter under soft switching in the whole operating range,” IEEE Trans. Power Electron., vol. 26, no. 4, pp. 1228–1236, Apr. 2011.

[6] H.Baiand C.Mi,“Eliminate reactive power and increase system efficiency of isolated bidirectional dual-active-bridge dc–dc converters using novel dual-phase-shift control,” IEEE Trans. Power Electron., vol. 23, no. 6, pp. 2905–2914, Nov. 2008.

[7] K. Wu, C. W. de Silva, and W. G. Dunford, “Stability analysis of isolated bidirectional dual active full-bridge dc-dc converter with triple phase-shift control,” IEEE Trans. Power Electron., vol. 27, no. 4, pp. 2007–2017, Apr. 2012.

[8] B. Zhao, Q. Song, W. Liu, G. Liu, and Y. Zhao, ‘‘Universal high-frequency-link characterization and practical fundamental-optimal strategy for dual-active-bridge DC-DC converter under PWM plus phase-shift control,’’ IEEE Trans. Power Electron., vol. 30, no. 12, pp. 6488–6494, Dec. 2015.

[9] W. Choi, K.-M. Rho, and B.-H. Cho, ‘‘Fundamental duty modulation of dual-active-bridge converter for wide-range operation,’’ IEEE Trans. Power Electron., vol. 31, no. 6, pp. 4048–4064, Jun. 2016.

[10] H. Shi, H. Wen, J. Chen, Y. Hu, L. Jiang, and G. Chen, ‘‘Minimum-reactive power scheme of dual-active-bridge DC–DC converter with three-level modulated phase-shift control,’’ IEEE Trans. Ind. Appl., vol. 53, no. 6, pp. 5573–5586, Nov. 2017.

[11] A. K. Jain and R. Ayyanar, ‘‘PWM control of dual active bridge: Comprehensive analysis and experimental verification,’’ IEEE Trans. Power Electron., vol. 26, no. 4, pp. 1215–1227, Apr. 2011.

[12] J. Huang, Y. Wang, Z. Li, and W. Lei, ‘‘Unified triple-phase-shift control to minimize current stress and achieve full soft-switching of isolated bidirectional DC-DC converter,’’ IEEE Trans. Ind. Electron. , vol.63,no.7, pp. 4169–4179, Jul. 2016.

[13] N. Hou, W. Song, and M. Wu, ‘‘Minimum-current-stress scheme of dual active bridge DC–DC converter with unified phase-shift control,’’ IEEE Trans. Power Electron., vol. 31, no. 12, pp. 8552–8561, Dec. 2016.

[14] A. Tong, L. Hang, G. Li, X. Jiang, and S. Gao, ‘‘Modeling and analysis of a dual-active-bridge-isolated bidirectional DC/DC converter to minimize RMS current with whole operating range,’’ IEEE Trans. Power Electron., vol. 33, no. 6, pp. 5302–5316, Jun. 2018.

[15] G. Jean-Pierre, M Khayamy, N. Altin, A. El Shafei, and A. Nasiri, “A Triple Phase-Shift Based Control Method for RMS Current Minimization and Power Sharing Control for Input-Series Output-Parallel Dual Active Bridge Converter,” IEEE Transportation Electrification Conference and Expo, Chicago, IL, 2020, pp. 1-6.

[16] K. Venkatachalam, C. Sullivan, T. Abdallah, and H. Tacca, “Accurate prediction of ferrite core loss with nonsinusoidal waveforms using only Steinmetz parameters,” in Proc. of IEEE Workshop on Computers in Power Electronics, Jun. 2002, pp. 36–41.

[17] J. Kennedy and R. Eberhart, “Particle swarm optimization,”in Proc. IEEE Int. Conf. Neural Netw. , Perth, WA, Australia, 1995, vol.4, pp.1942–1948.